Link Adaptation for Mitigating Earth-to-Space Propagation Effects on the NASA SCaN Testbed

Deirdre K. Kilcoyne
Hume Center, Virginia Tech
1991 Kraft Dr.
Blacksburg, VA 24061
dkilcoyne@vt.edu

William C. Headley
Hume Center, Virginia Tech
1991 Kraft Dr.
Blacksburg, VA 24061
cheadley@vt.edu

Zach J. Leffke
Hume Center, Virginia Tech
1991 Kraft Dr.
Blacksburg, VA 24061
zleffke@vt.edu

Sonya A. Rowe
Hume Center, Virginia Tech
1991 Kraft Dr.
Blacksburg, VA 24061
sarowe@vt.edu

Dale J. Mortensen
NASA Glenn Research Center
21000 Brookpark Rd
Cleveland, OH 44135
dale.mortensen@nasa.gov

Richard C. Reinhart
NASA Glenn Research Center
21000 Brookpark Rd
Cleveland, OH 44135
richard.c.reinhart@nasa.gov

Robert W. McGwier
Hume Center, Virginia Tech
1991 Kraft Dr.
Blacksburg, VA 24061
rwmcgwi@vt.edu

***Abstract*—In Earth-to-Space communications, well-known propagation effects such as path loss and atmospheric loss can lead to fluctuations in the strength of the communications link between a satellite and its ground station. Additionally, the typically unconsidered effect of shadowing due to the geometry of the satellite and its solar panels can also lead to link degradation. As a result of these anticipated channel impairments, NASA's communication links have been traditionally designed to handle the worst-case impact of these effects through high link margins and static, lower rate, modulation formats. The work presented in this paper aims to relax these constraints by providing an improved trade-off between data rate and link margin through utilizing link adaptation. More specifically, this work provides a simulation study on the propagation effects impacting NASA's SCaN Testbed flight software-defined radio (SDR) as well as proposes a link adaptation algorithm that varies the modulation format of a communications link as its signal-to-noise ratio fluctuates. Ultimately, the models developed in this work will be utilized to conduct real-time flight experiments on-board the NASA SCaN Testbed.**

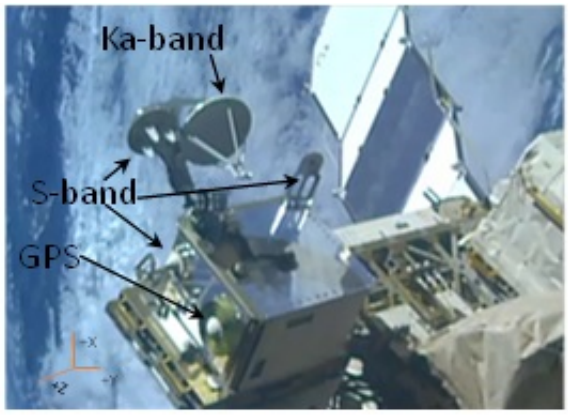

Figure 1. NASA SCaN Testbed on-board the ISS.

TABLE OF CONTENTS

1. INTRODUCTION

Traditionally, NASA communication links have been designed to operate during the worst-case, anticipated propagation conditions. These communication links are generally configured with a fixed data rate, a static modulation and/or coding scheme, and high link margins to communicate during the worst-case scenario. This approach often results in an underutilized system and limits flexibility during a variety of receiving scenarios.

This worst-case planning approach ensures that communication links are maintained during even the worst expected Earth-to-Space propagation effects. These propagation effects include path loss, atmospheric loss, attenuation due to rain, and ionospheric loss, among others [1]. Another consideration that can affect these communication links is antenna obstruction by either the satellite's body or its solar panels [2]. These effects can be detrimental to a communications link if the link margin drops below the accepted threshold for the transmitting waveform.

In the future, NASA envisions a more dynamic, flexible, and efficient communications network which optimizes mission data returns while minimizing the burden and cost of spacecraft resources. As a step towards these goals, this paper proposes a link adaptation (LA) technique for the Earth-to-Space communications link between the NASA Space Communications and Navigation (SCaN) Testbed and the Glenn

Research Center (GRC) ground station. LA is a method used to monitor and switch modulation schemes depending on the strength of the communication link. Common types of LA that have been discussed are adaptive coding and modulation (ACM) as well as adaptive power allocation (APA) [3–5].

LA has been used for a variety of terrestrial applications over the years such as WiFi, land mobile communications, and cellular systems [3–8]. LA has also been used in satellite communications applications [9–12]. These contributions evaluate the performance of an adaptive modulation system in the unique space-based propagation environment. However, they either present LA in a broadcasting system with no feedback to the ground station or do not consider shadowing effects.

First, this work will model and evaluate the point-to-point propagation path for the SCaN Testbed on-board the International Space Station (ISS), considering common effects such as path loss and atmospheric loss, as well as shadowing effects its antenna experiences as a result of the ISS body or its solar panel. Next, a LA waveform algorithm is developed to operate the uplink path at a modulation and data rate scheme to maximize the data throughput. Through simulation analysis, it is shown that the developed algorithm balances the trade-off between the bit error rate and data rate as a function of the modulation scheme.

Ultimately, given that the NASA's SCaN Testbed on the ISS provides an ideal test environment for new satellite communication waveforms for NASA, the results of this work will be validated by an on-flight experiment on the testbed as future work.

2. THE NASA SCAN TESTBED

SCaN Testbed Background and Overview

The NASA SCaN Testbed consists of three SDRs, one at Ka-band and two at S-band. Each SDR can be reprogrammed with custom software for almost any desired waveform characteristic, making it ideal for this work. Positioned on the external truss of ISS, the SCaN Testbed has views to NASA's relay satellites, called the Tracking and Data Relay Satellite System (TDRSS), and direct-to-ground stations. Fig. 1 shows the SCaN Testbed aboard the ISS at an experiment payload site. Only the antennas are visible in the picture, as the SDRs themselves are within the flight enclosure.

Two of the antennas, one at Ka-band and one at S-band, share a gimbal mount and are used to track TDRSS satellites. There are two fixed S-band antennas, one facing zenith (+z) and one facing the direction of travel (+x). A second fixed antenna is visible on the zenith side for reception of GPS signals. The ram-facing antenna is the focus of this work, as it communicates directly with a ground station at GRC. This fixed, wide-angle antenna provides four to six minute contacts with the ground station during each pass.

The S-band station at GRC, shown in Fig. 2, features a 2.4m parabolic antenna, tracking software, and is fully networked into the SCaN Testbed's operations center. As the GRC station serves as the transmitter in this work, all calculations and models are performed with the parameters of this S-band configuration.

Figure 2. **S-band Ground Station at GRC.**

Satellite SDR Overview

The testbed SDR being used for this work's modeling and simulation (and future on-flight testing) is an S-band transceiver with several reconfigurable components. The radio has both a general purpose processor (GPP) and field programmable gate arrays (FPGAs) to perform waveform application operations. The GPP and two Xilinx Virtex II FPGAs are the user-programmable components that will host the algorithm and receiver for this work. As such, this work will take the component specifications into consideration during the development. Additionally, a ground version of the SDR exists at GRC for functional development testing. This prototype unit will be leveraged for initial waveform application radio integration prior to on-orbit flight testing.

GRC Ground Station Overview

A variety of direct-to-ground experiments were the driving force for the GRC Ground Station development. Coming online in early 2015, the facility is intended to serve research initiatives that increase the communication capabilities of NASA. The antenna tracking and RF subsystems are therefore designed to handle the associated slew rates, signal power changes, and Doppler variations expected for LEO-to-ground links that are discussed in detail in Section 4. The antenna-pointing system is capable of operating closed-loop or open-loop, with ephemeris data of the spacecraft as the starting point. Closed-loop tracking uses the received power level to adjust the pointing. Direct line of sight contacts can have a peak duration of roughly 6.5 minutes, which is depicted in the simulations presented in Section 6.

GRC-developed software tools perform the orbital predictions and transform these to the antenna pointing and tracking commands. Another software tool is used to estimate several system parameters for the communications link including: contact times, power levels, BER performance, and ISS link obscuration. This flight data will be used as a metric to measure this work's performance.

3. COMMUNICATIONS LINK CONFIGURATION

The configuration of the communications link modeled and analyzed in this work is depicted in Fig. 3. The Experimental Path Uplink consists of an adaptive transmitter with several possible modulation modes. These modulation schemes are BPSK, QPSK, 8-PSK, 16-QAM, and 64-QAM. The receiver on-board the SCaN Testbed, to be designed with results from

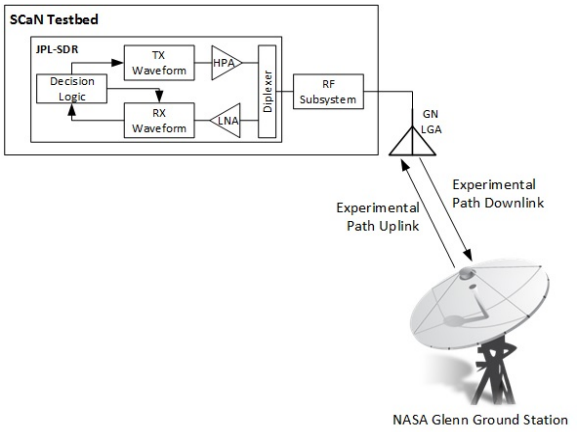

Figure 3. System Block Diagram.

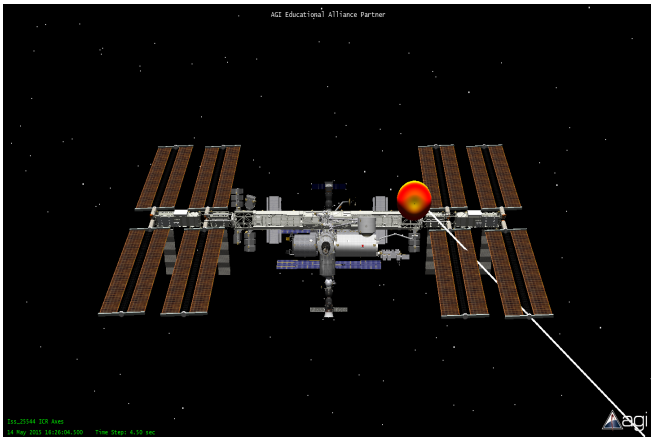

Figure 4. Flight Antenna Obstructed by Solar Panels.

this work in mind, will receive the data and then perform signal-strength analysis. Depending on the strength of the received signal, the link adaptation algorithm discussed in Section 5 may determine that a different modulation scheme should be transmitted. For example, if the ground station is transmitting 16-QAM on the uplink and the solar panel rotates to a position that obscures the antenna, the received signal energy will decrease. If the change in measured received energy results in an increase of the anticipated BER past a pre-determined threshold, the decision logic will determine a new modulation scheme that stays within the BER threshold at the current received energy. In this example, the logic would determine that a lower-order modulation scheme, such as QPSK, would ensure the desirable BER. The Experimental Path Downlink seen in Fig. 3 then provides feedback on the desired modulation scheme to the ground station via a high-fidelity BPSK transmitter. The transmitter at the ground station then switches to transmitting the requested modulation scheme and continues to transmit data. While the transmitter transitions to the updated modulation scheme, the receiver on-board the SDR will also reconfigure to receive the newly expected modulation scheme. The receiver will wait a predetermined time, based on the channel delay, for the transmitter to switch modulation schemes and resume transmission on the communications link.

4. Propagation Analysis

The propagation environment of the communications link described in Section 3 must be modeled in order to develop the LA algorithm. This section discusses the tools applied in this analysis. It also presents calculations of an estimated link budget. Due to the export-controlled nature of this work, some parameters within the analysis are estimated or approximated by similar prior work to present the function of the proposed LA system without compromising propriety information.

Systems Toolkit

This project utilizes the Analytical Graphics, Inc. (AGI) Systems Toolkit (STK) software for modeling the communication link. STK has a MATLAB interface capability, which enables users to instantiate satellites, ground stations, receivers, antennas, etc. and then perform analysis on these objects from MATLAB. The STK interface was used to set-up the ISS, ground station, SCaN testbed receiver, and antenna and then calculated accesses, or times during which the satellite is visible to the ground station. The data provided from these STK simulations were loaded into MATLAB for further calculation.

Table 1. STK Parameters Applied in Analysis.

Access Parameters
Access Number
Epoch Time (sec)
Range (km)
Range Rate (km)
Azimuth (deg)
Elevation (deg)
Receiver Gain Matrix (dB)
Solar Panel Obstruction
Epoch Time (sec)
Percent Obscured Area

STK provided many of the simulated values in the propagation analysis. Table 1 displays a summary of these values. Most notably, STK was used to determine the times during which the solar panel rotated in front of the antenna. As an example, Fig. 4 is an STK illustration of the solar panel blocking the line-of-sight of the SCaN testbed antenna to the ground station. The antenna pattern used in this figure is a generic STK-provided antenna pattern GPS FRPA. This antenna pattern was substituted in place for the flight SDR antenna pattern, due to export-control restrictions. This antenna pattern gives a more realistic model of the anticipated receiver gains as it varies with both azimuth and elevation.

Path Loss

Path loss is an important consideration in a satellite communications link budget as it introduces a variable received signal power across each satellite pass. With each access having a different path loss curve, many values of received signal strength are experienced by the flight SDR on board the ISS. Range data from STK analysis was used to estimate the range value used in calculating path loss. Fig. 5 displays how the path loss changes over time for a representative 60 out of the 207 accesses over a month period. This path loss graph depicts the entirety of the pass that the ISS is visible to the ground station; however the flight SDR will not have the same visibility times due to the fixed directional antenna.

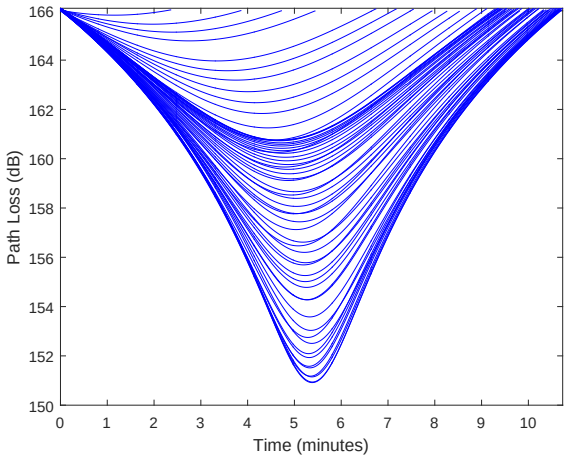

Figure 5. Time-Varying Path Loss for 60 Accesses.

The path loss values found in Fig. 5 are calculated through

$$L_P = 10\log_{10}\left(\frac{4d\pi}{\lambda}\right)^n, \quad (1)$$

using the path loss characteristics in Table 2. Additionally, the maximum and minimum path losses values were calculated and are also summarized in Table 2.

Link Budget

The ground station transmitting antenna's gain is given by

$$G_{TX} = 10\log_{10}\left(\eta\left(\frac{d\pi}{\lambda}\right)^2\right), \quad (2)$$

using the antenna characteristics defined in Table 2. Given an approximated efficiency of 70%, a commonly accepted efficiency for a well-designed and optimized parabolic antenna [13], the gain was found to be approximately 32.5 dBi.

Before manipulating the total link budget with additional propagation effects such as shadowing, a base-line link budget is first calculated. For this analysis, a worst-case calculation is performed, using the maximum path loss and worst receiver gain.

First, the Effective Isotropically Radiated Power (EIRP) is found to be 40.5 dBW using the parameters of the transmitting ground station defined in Table 2 through

$$\text{EIRP}_{TX} = P_{TX} + G_{TX} - L_{TX}. \quad (3)$$

Following the calculation of the EIRP_{TX}, the received power is calculated through

$$P_{RX}[\text{dBW}] = \text{EIRP}_{TX} - L_P - L_{atmo} - L_{iono} + G_{RX}, \quad (4)$$

where the receiver antenna gain, G_{RX}, is dependent on the azimuth and elevation of the satellite as it passes over the ground station due to a fixed, known pointing angle. Using STK, a matrix of receiver antenna gain values are generated for azimuth values between -180 and 180 degrees and elevations between -90 and 90. In simulations of each access, the receiver gain is selected from the matrix and correlated to the azimuth and elevation values from the STK access analysis.

Table 2. Summary of Propagation Analysis Characteristics and Calculations.

Path Loss Characteristics			
		Minimum	Maximum
d	Range	396.88 km	2328.67 km
λ	Wavelength	0.14 m	0.14 m
n	Free-space Loss Exponent	2	2
L_P	Path Loss	150.7 dB	166.1 dB
GRC Ground Station Specifications			
f	S-band Frequency		2.07 GHz
P_{TX}	Transmitter Power		10 W
R_S	Symbol Rate		2.0 MSps
d	Antenna Diameter		2.4 m
η	Efficiency		70%
Transmitter Antenna Gain			
η	Efficiency		70%
d	Antenna Diameter		2.4 m
λ	Wavelength		0.14 m
G_{TX}	Transmitter Antenna Gain		32.5 dBi
Effective Isotropically Radiated Power (EIRP)			
P_{TX}	Transmitter Power		10 dBW
G_{TX}	Transmitter Antenna Gain		32.5 dBi
L_{TX}	Transmitter Losses (estimated)		2 dB
EIRP_{TX}	EIRP		40.5 dBW
Received Power Worst-Case			
EIRP_{TX}	EIRP		40.5 dBW
L_P	Path Loss		166.1 dB
L_{atmo}	Atmospheric Loss		1 dB
L_{iono}	Ionospheric Loss		1 dB
G_{RX}	Receiver Antenna Gain		-6.5 dBi
P_{RX}	Received Power		-134.1 dBW
System Temperature			
T_{ref}	Reference Temperature		290 K
NF_{dB}	Noise Figure		5 dB
T_{RX}	Receiver Temperature		432.5 K
T_{ant}	Antenna Temperature (estimated)		200 K
T_{sys}	System Temperature		632.5 K
Noise Power			
k	Boltzmann's Constant		1.39×10^{-23} J/K
T_{sys}	System Temperature		632.5 K
B_n	Noise Bandwidth		2 MHz
Doppler Frequency			
		Minimum	Maximum
f_0	Emitted Frequency	2.07 GHz	2.07 GHz
c	Velocity of Waves in Free Space	3×10^8 m/sec	3×10^8 m/sec
v_r	Velocity of Receiver	-6.8 km/sec	+6.8 km/sec
f	Doppler Frequency	-50 kHz	+50 kHz

Next, the noise power is determined through

$$P_n[\text{dBW}] = k + T_{sys} + B_n, \quad (5)$$

where the noise bandwidth B_n is equivalent to the system symbol rate, as root raised cosine filtering is assumed at the receiver [14].

Common receivers have a noise figure of 3 dB [15]. The noise figure of the flight SDR is thus conservatively estimated at 5 dB, to overestimate the actual noise figure. The antenna temperature is conservatively estimated at 200 K [16] to calculate the system noise temperature for the noise power in the link budget. Using the system temperature values listed in

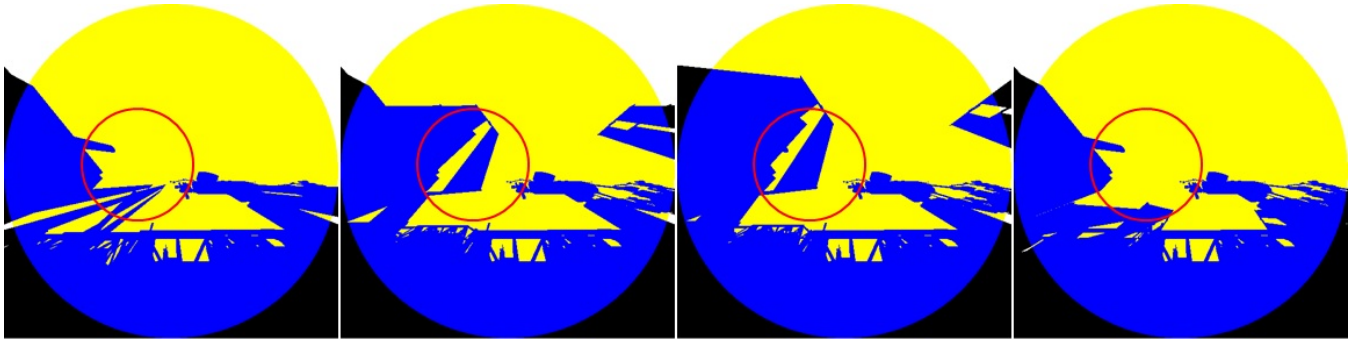

Figure 6. STK Obscuration Tool Showing Stages of a Solar Panel Rotation.

Table 3. Summary of Relevant C/N Parameters.

Link Budget		
P_{RX}	Received Power	-134.1 dBW
k	Boltzmann's Constant	-228.6 dBW/(dBK/Hz)
T_{sys}	System Temperature	28 dBK
B_n	Noise Bandwidth	63 dBHz
C/N	Carrier-to-Noise Ratio	4 dB

Table 2, the receiver noise temperature is calculated through

$$T_{RX}[K] = T_{ref}\left(10^{\frac{NF_{dB}}{10}} - 1\right). \quad (6)$$

Given (6) and the approximated T_{ant}, the system temperature is determined by

$$T_{sys}[\text{dBK}] = 10\log_{10}\left(T_{ant} + T_{RX}\right). \quad (7)$$

The final step in the link budget is the calculation of carrier-to-noise ratio. Given the received power (4) and noise power (5), the carrier-to-noise ratio is calculated by

$$C/N[\text{dB}] = P_{RX} - P_n. \quad (8)$$

The baseline carrier-to-noise ratio, using the maximum worst-case scenario for path loss, is shown in Table 3.

Finally, in order to perform LA analysis as a function of bit error rates in the following, the carrier-to-noise ratio is related to the received energy per symbol through

$$\frac{E_s}{N_0} = \frac{CT_sB_n}{N}. \quad (9)$$

In ideal conditions, the carrier-to-noise ratio and E_s/N_0 are equivalent due to the fact that T_sB_n = 1, $T_s = \frac{1}{R_s}$, and $B_n = R_S$ [14]. Therefore, for this work, the following relation is used:

$$\frac{E_s}{N_0} = \frac{C}{N} \quad (10)$$

Shadowing

Prior work has shown that an antenna blocked by solar panels experiences a degradation loss of 6 dB during a time of solar panel shadowing [17]. While this prior work investigated an antenna with different pattern characteristics, a similar approach can be applied to this work. In other words, here a similar method of simulating a fixed degradation as a result of shadowing is included in the link budget analysis for the LA algorithm development.

The STK obscuration tool was used to determine the position of the solar panels and whether they are blocking the S-band antenna. A recent work applied the STK obscuration tool in an assessment of ENVISAT antenna obstruction [2] by leveraging the tool's percentage of field-of-view that is obstructed. This tool shows the percentage of the view down the antenna's boresight that is blocked by either the solar panel or the body of the ISS. Fig. 6 depicts a few examples of this tool at discrete time steps, during which the solar panel rotates through the field of view. For this work, the access is classified as shadowed and the link budget includes a shadowing loss in the calculation if the percent obscured rise above a threshold of 45%. The shadowing loss is a function of the obstruction percentage, with the maximum measured at 9.8 dB. This value is a conservative estimate based upon [17].

Doppler Shift

Doppler shift is another time-varying parameter that needs to be addressed in the uplink. While this consideration does not need to be included in the overall link budget analysis, it does need to be addressed in order to avoid frequency drifts/offsets. Because Doppler shift can be calculated before a link is established with the satellite, it is assumed here that the ground station transmitter will adjust for the shift as communication begins. Consideration for Doppler at the ground station will relax the design requirements for the flight SDR. The Doppler shift will be calculated before the pass begins using data from STK. STK returns range rate for each time step in the satellite's pass allowing the Doppler shift to be calculated by

$$f = \left(\frac{c + v_r}{c}\right) f_0. \quad (11)$$

Fig. 7 depicts the anticipated Doppler shift for the first 60 accesses of the month's simulation. Because the transmitter on the ground will be adjusting for the Doppler shift, instead of the receiver, the Doppler graph for analysis is inverted from the typical Doppler graph.

5. Link Adaptation Algorithm

The system design of the LA algorithm consists of MATLAB simulation using data from the propagation analysis

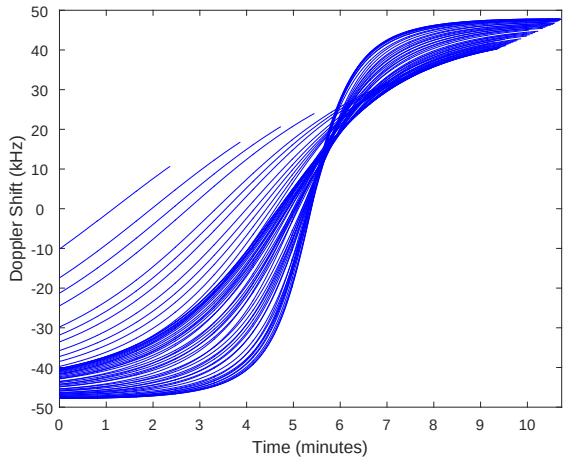

Figure 7. Time-Varying Doppler shift for 60 accesses.

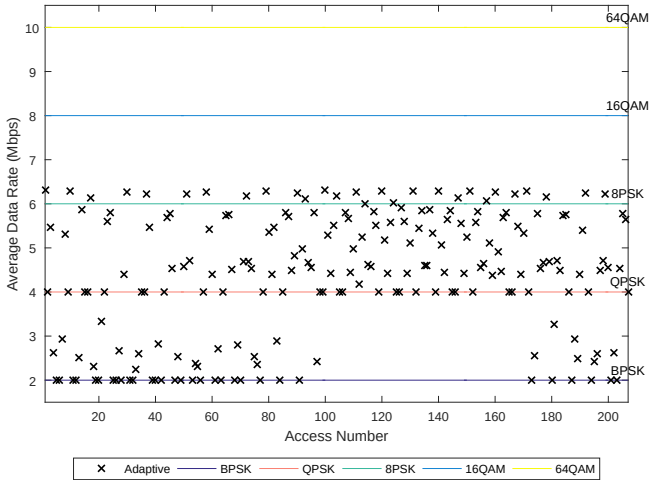

Figure 8. Bit Rate of Adaptive and Constant Modes.

Table 4. Bit Error Rate Curves

Bit Error Rate Calculations for Considered Modulations.	
BPSK	$P_b = Q\left(\sqrt{\frac{2E_s}{N_0}}\right)$
MPSK	$P_b = \frac{2}{\log_2 M} Q\left(\sqrt{\left(\sin\frac{\pi}{M}\right)^2 \frac{E_s}{N_0}}\right)$
MQAM	$P_b = \frac{4}{\log_2 M}\left(1-\frac{1}{\sqrt{M}}\right) Q\left(\sqrt{\frac{3}{M-1}\frac{E_s}{N_0}}\right)$
	where M is number of bits/symbol

in Section 4. For the purpose of simulation, a trigger for when shadowing occurred was implemented as previously described. For this work, the BER is used as the decision metric for modulation switching. The BERs are calculated using the equations defined in Table 4 [18]. These equations are defined in terms of the received E_s/N_0, defined here by 9, in order to distinguish the inherent energy increase necessary between BPSK and QPSK. Therefore, decision metrics can be based off of the received E_s/N_0, as the BERs are a function of this parameter.

Given that the switching algorithm operates as a function of the output BER, so it can serve a variety of coded or uncoded systems. The BER equations presented in Table 4 are defined assuming an uncoded system. The application of forward error correction (FEC) encoding would decrease the required E_s/N_0 to achieve the same BER as an uncoded system but the algorithm would continue to switch modulation schemes as the effectove BER exceeds the threshold.

For this work, BER calculations made for simple comparisons between modulation schemes, in which all E_s/N_0 values were determined before analysis. However, in practice onboard the SCaN Testbed receiver measurement of bit error rates will not be available, as bit throughput for this configuration is not enough to accurately determine BER. Thus, an ability to measure performance in realtime is necessary to determine modulation switching. Error vector magnitude calculations (EVM) will provide this capability. EVM measures the symbol offset from the expected symbol. The measurement of carrier-to-noise ratio from the link budget calculations defined by (8) can be used to estimate EVM and check EVM measurement performance. Thus, the BER

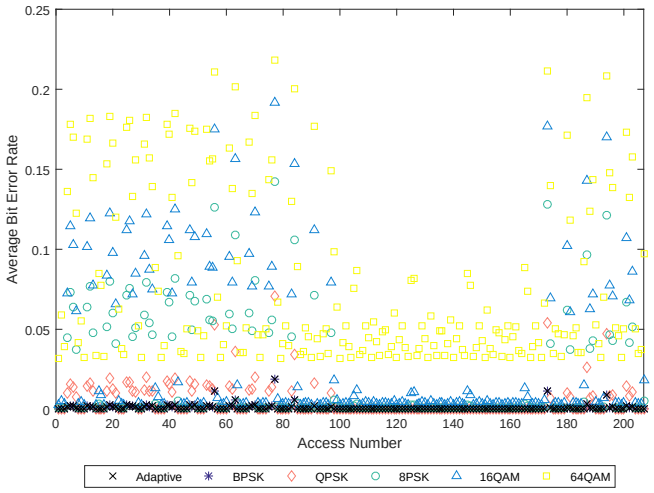

Figure 9. BER of Adaptive and Constant Modes.

will be derived from the EVM calculation rather than the theoretical equations in Table 4 [19]. EVM will provide similar observation of the BER in relation to a selected threshold and will switch as necessary. For the purposes of this simulation, the BER threshold is 10^{-5}. TDRSS operates at 10^{-5} or less, so this selection aligns with current NASA operations.

6. Simulation Results

Simulation Set-up

The simulation to be discussed is derived from a one-month simulation within STK. Range rate, range, elevation, and azimuth were all calculated from STK's internal report generator at 1 second timesteps. All data was exported from the STK interface and manipulated in MATLAB. During this one-month time period, the flight SDR was visible to the ground station 207 times, all with varying lengths of visibility. The briefest ground-to-ISS access was 0.2 minutes and the longest was 10.8 minutes.

Fig. 8 depicts the average bit rate of every pass in this month-long scenario. Each of the modulation scheme bit error rate reference lines are plotted to compare bit rate against

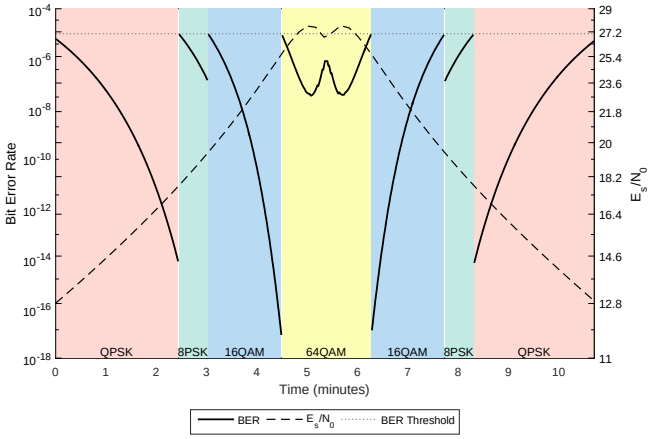

Figure 10. BER and E_s/N_0 for Access 1

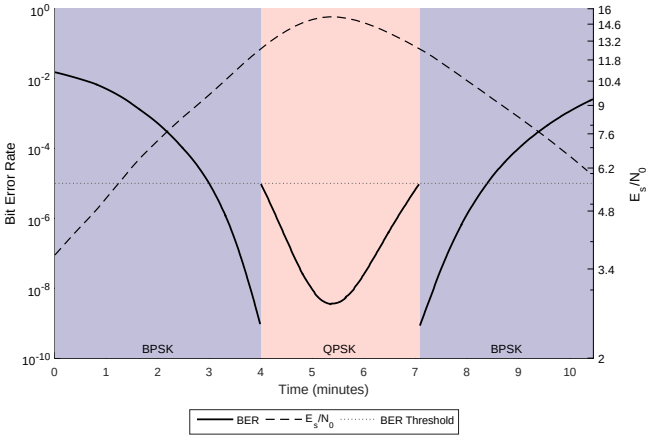

Figure 11. BER and E_s/N_0 for Shadowed Access 196

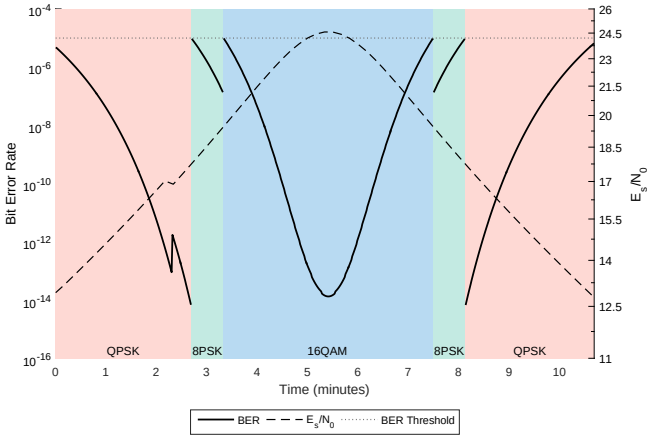

Figure 12. BER and E_s/N_0 for Access 107

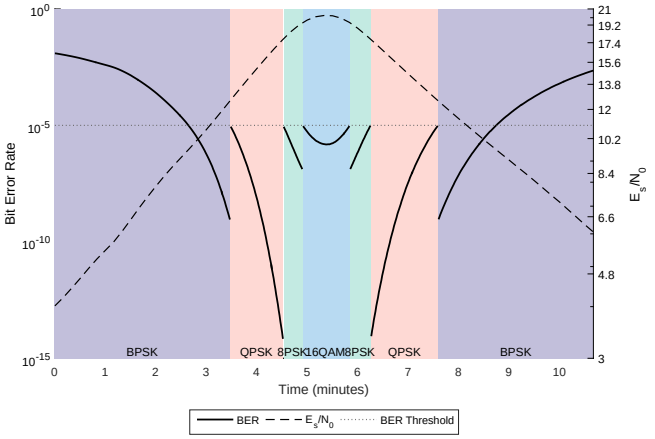

Figure 13. BER and E_s/N_0 for Shadowed Access 181

constant modulation schemes. Additionally, Fig. 9 depicts the average BER for the adaptive receiver and each of the constant modulation schemes. Fig. 8 and Fig. 9 show that, while the data rate would always be maximized with sending 64-QAM, oftentimes, a receiver operating at constant 64-QAM is significantly exceeding the BER threshold.

For every access, the resulting symbol energy per noise ratio is calculated using (9) and the bit error rates for all the potential modulation schemes (BPSK, QPSK, 8PSK, 16-QAM, 64-QAM) are determined using Table 4. The bit error rate values are compared to the threshold (in this simulation 10^{-5}) and the highest order modulation scheme that falls under the threshold is selected as the current modulation scheme.

Figs. 10-13 show a sampling of the accesses in this simulation. Each of these accesses depict a gradual shift between modulation schemes because the STK obscuration tool provides a linear characterization of the solar panel shadowing. It is expected that the on-orbit simulation will have sharper transitions and degradations and thus will not gradually transition through modulation schemes. Fig. 10 depicts the first access in which the pass starts low and then increases enough in signal strength that 64-QAM can be transmitted. Fig. 11 depicts a bad shadowing condition, in which BPSK is transmitted but the BER is still vastly above the desired rate. However, once the signal energy increases enough, the receiver is able to switch up to QPSK for a period of time. On the descent of the ISS, the curve of the E_s/N_0 is not symmetrical due to the roll-off of the receiver antenna gain.

Fig. 12 depicts another non-shadowed pass that does not reach a high enough E_s/N_0 to switch to 64-QAM, however, 16-QAM can be received for an extended period during this pass. The discontinuity in the QPSK curve is a result of the receiver gain matrix; the azimuth and elevation at that point in the pass correlate to a decrease in the receiver antenna gain. Fig. 13 depicts another access that is experiencing solar panel shadowing. This shows that the algorithm will not always be able to keep the BER below the desired rate; especially when the ISS first is visible to the ground station. Fig. 13 demonstrates that the adaptive modulation can be applied during periods of solar panel shadowing, although on the ends of the pass, BPSK must be transmitted in order to keep the BER as close to the threshold as possible.

7. CONCLUSION

The work presented in this paper has shown that an adaptive modulation receiver will perform better than fixed-modulation in optimizing data throughput while minimizing the bit error rate on-board NASA's SCaN Testbed. This was done by first analyzing the propagation effects experienced by the NASA's SCaN Testbed on-board the ISS. Next, the propagation analysis was used to develop an adaptive modulation switching algorithm that monitors the bit error rate of the system and adapts accordingly. The simulations of this algorithm using the propagation environment of the

Testbed demonstrate that a properly implemented adaptive modulation receiver can provide a better trade-off between BER and throughput, finding an optimum configuration. This algorithm improves upon NASA's traditional communication approach by maintaining data transmission during times of decreased link quality, albeit at a lower throughput.

Given the successful results of this work, an on-orbit test onboard the ISS is planned to test the performance of the LA algorithm in-flight. Adaptive data rate links are the first step towards a more intelligent system. Coupling cognition with these adaptive waveforms will provide even more efficiency for the communication links. Applications will monitor and learn link behavior, predict propagation losses, recognize and avoid interference, and cooperatively use the spectrum. Capabilities such as these would increase the amount of science data returned from NASA missions in the future.

8. Future Work

In practice, due to estimation error, the simulated algorithm-could oscillate between modulation schemes if the estimated E_s/N_0 is on the boundary between modulation schemes. This fluctuation between modulation schemes would incur significant down-time for the receiver as it waited for the transmitter to switch multiple times in a short period. Each receiver switch introduces a link delay while the transmitter shifts schemes and retransmits data. When using the EVM measurement technique, a buffer will be defined in order to prevent oscillation between modulation schemes. The oscillation buffer will work to balance the goal of continuous data transmission and maintaining the bit error rate threshold.

References

[1] A. Arun and T. Sreeja, "An effective downlink budget for 2.24 ghz s-band LEO satellites," in *Information & Communication Technologies (ICT), IEEE Conference on*, pp. 342–345, Apr. 2013.

[2] J. Deloo, "Analysis of the rendezvous phase of e.deorbit," Master's Thesis, TU Delft, Delft University of Technology, Jan. 2015.

[3] K. Baum, T. Kostas, P. Sartori, and B. Classon, "Performance characteristics of cellular systems with different link adaptation strategies," *Vehicular Technology, IEEE Transactions on*, vol. 52, no. 6, pp. 1497–1507, Nov. 2003.

[4] E. Armanious, D. Falconer, and H. Yanikomeroglu, "Adaptive modulation, adaptive coding, and power control for fixed cellular broadband wireless systems: some new insights," in *Wireless Communications and Networking, IEEE*, vol. 1, pp. 238–242, March 2003.

[5] N. Mehta and A. Goldsmith, "Performance analysis of link adaptation in wireless data networks," in *IEEE Global Telecommunications Conference*, vol. 3, pp. 1422–1426, Apr. 2000.

[6] S. Ci and H. Sharif, "An link adaptation scheme for improving throughput in the IEEE 802.11 wireless LAN," in *Local Computer Networks, Proceedings, 27th Annual IEEE Conference on*, pp. 205–208, Nov. 2002.

[7] Z. Katona and J. Bito, "Performance of link adaptation techniques for different service classes through land mobile satellite communication channels," in *Satellite and Space Communications, 2006 International Workshop on*, pp. 105–109, Sept. 2006.

[8] M. Bergmann, W. Gappmair, and O. Koudelka, "Parameter estimation for link adaptation on land-mobile satellite links," in *Communication Systems, Networks, Digital Signal Processing (CSNDSP), 9th International Symposium on*, pp. 1139–1143, July 2014.

[9] S. Boyd and T. Macdonald, "Satellite communications link adaptation design and interaction with TCP," in *Military Communications Conference*, vol.4, pp. 2042–2047, Oct. 2005.

[10] T. El Shabrawy and S. Wahed, "Adaptive modulation and coding for broadcast DVB-H systems," in *Personal, Indoor and Mobile Radio Communications, IEEE 20th International Symposium on*, pp. 1292–1296, Sept. 2009.

[11] C. Morel, P. D. Arapoglou, M. Angelone, and A. Ginesi, "Link adaptation strategies for next generation satellite video broadcasting: A system approach," *Broadcasting, IEEE Transactions on*, vol.61, no.4, pp.603-614, Dec. 2015

[12] L. Abderrahmane, D. Hamed, and M. Benyettou, "Design of an adaptive communication system for implementation on board a future Algerian LEO satellite," in *Aerospace Conference, 2008 IEEE*, pp. 1–5, March 2008.

[13] A. D. Monk, "Antennas and arrays," in *Electronics Engineer's Reference Book*, F. F. Mazda, Ed., p. 49/9.

[14] T. Pratt, C. Bostian, and J. Allnutt, *Satellite Communications*, 2nd ed.

[15] K. R. Sturley, "Noise and communication," in *Electronics Engineer's Reference Book*, F. F. Mazda, Ed., p. 51/5.

[16] S. Cakaj, B. Kamo, I. Enesi, and O. Shurdi, "Antenna noise temperature for low earth orbiting satellite ground stations at l and s band," in *SPACOMM: The Third International Conference on Advances in Satellite and Space Communications*, 2011.

[17] G. Paynter, W. Burnside, and T. Lee, "A systematic approach to design and analysis of antennas on complex platforms," *Antennas and Propagation Magazine, IEEE*, vol. 43, no. 6, pp. 38–44, Dec. 2001.

[18] J. G. Proakis and M. Salehi, *Digital Communications*, 5th ed.

[19] R. Shafik, S. Rahman, and R. Islam, "On the extended relationships among EVM, BER and SNR as performance metrics," in *Electrical and Computer Engineering, International Conference on*, pp. 408–411, Dec 2006.

BIOGRAPHY

Deirdre K. Kilcoyne *is a second-year Master's of Science student from the Electrical and Computer Engineering department at Virginia Tech. She works as a member of the graduate research team at the Virginia Tech Ted and Karyn Hume Center under her advisor Dr. Robert W. McGwier.*

Robert W. McGwier *is the Director of Research for the Ted and Karyn Hume Center for National Security and Technology, and joined the Virginia Tech faculty in 2011. He received his Ph.D. in applied mathematics from Brown University in 1988. McGwier has served on the board of directors of AMSAT, Inc. for multiple two-year terms. During 2006-2008 Dr. McGwier served as AMSAT's VP for engineering during the period when AMSAT designed and flew the ARISS on the ISS as well as Suitsat and ARISSAT.*

William C. Headley *is a Research Associate with the Ted and Karyn Hume Center for National Security and Technology at Virginia Tech. He earned his PhD in Electrical and Computer Engineering from Virginia Tech under the schools prestigious Bradley Fellowship. Through his graduate studies and onwards, signal detection, signal classification, and signal parameter estimation have been an area of focus in his research.*

Zachary Leffke *is a Research Associate at the Hume Center for National Security and Technology. Mr. Leffke is a former United States Marine and served as a Ground Mobile Forces Satellite Communications Operator while on Active Duty. Upon his End of Active Service from the USMC he earned his BSEE and MSEE degrees from Virginia Tech. He is currently a Principal Investigator for the design and implementation of Virginia Tech's new Satellite Ground Station.*

Sonya Rowe *is a Project Manager with the Ted and Karyn Hume Center for National Security and Technology at the Virginia Polytechnic Institute and State University. She supports sponsored research programs for the Department of Defense and Intelligence Community. She received her M.S. in Strategic Intelligence from the National Defense Intelligence College. She is a Certified Associate in Project Management.*

Dale Mortensen *is an electronics engineer at the NASA Glenn Research Center (Cleveland, OH). He currently serves as the Cognitive Products lead for the Cognitive Communications Systems Project. He has served as the NASA liaison for Virginia Techs adaptive waveform switching experiment.*

Richard Reinhart *is a senior communications technologist with NASAs Glenn Research Center (GRC), located in Cleveland, Ohio. He currently serves as the Principal Investigator for NASAs software defined radio (SDR) flight experiment aboard ISS, called the SCAN Testbed - Space Communications and Navigation Testbed and a Principal Investigator of the Space Telecommunications Radio System (STRS) Architecture, flying for the first time in space in the SCaN Testbed SDRs.*